

# Seismic and gravity constraints on flexural models for the origin of seaward dipping reflectors

R.L. Morgan and A.B. Watts

*Department of Earth Sciences, South Parks Road, Oxford OX1 3AN, UK. E-mail: [rebecca.morgan@earth.ox.ac.uk](mailto:rebecca.morgan@earth.ox.ac.uk)*

Accepted 2018 June 20. Received 2018 May 11; in original form 2017 September 18

## SUMMARY

Seaward dipping reflectors (SDRs) are ubiquitous features of the offshore regions of volcanic rifted continental margins where they comprise wedge-shaped packages of mainly extrusive lava flows. However, their origin has been disputed with some workers suggesting they form by progressive subsidence of extended crust while others propose they are accommodated within the crust by one or more continent-dipping normal faults. We present here a simple model in which SDRs are formed by a succession of dykes which intrude and load the crust. These loads cause a surface flexure, which is subsequently infilled and loaded by volcanic material. The model, which does not require a bounding normal fault, explains the arcuate shape, limited offlap geometries and downdip thickening of SDRs as observed in seismic reflection profile data. By comparing observed and calculated dips we are able to constrain the elastic plate model type and the effective elastic thickness of extended lithosphere,  $T_e$ . Results suggest a broken plate or significantly weakened continuous plate model is required to produce the characteristic arcuate shape. Decreasing the  $T_e$  for successive loads as rifting progresses produces offlap of subpackages, while increasing the  $T_e$  produces onlap. We have verified our results using process-oriented gravity modelling, in which the gravity effect of surface volcanic infill loads is calculated and combined with the gravity effect of buried dyke loads and the gravity effect of their isostatic compensation. Results from a case study in the Orange Basin, offshore Namibia show good general agreement between observed Airy isostatic anomalies and calculated gravity anomalies with  $T_e$  in the range 1–3 km. The steep gradient that is often observed in the Airy isostatic gravity anomaly at rifted margins is therefore a useful proxy for the seaward edge of the dykes that intrude the crust prior to seafloor spreading, rather than a change in basement elevation at the boundary between oceanic and continental crust, as had been proposed by previous workers.

**Key words:** Gravity anomalies and Earth structure; Africa; Continental tectonics: extensional; Lithospheric flexure.

## INTRODUCTION

Volcanic rifted margins, which may comprise a majority of the world's rifted margins, are distinguished by their extrusive volcanism and intrusive magmatism at the time of continental break up (Hinz 1981; Mutter *et al.* 1982). The principal evidence for volcanism has come from seismic reflection and refraction profile data. Reflection data have revealed Seaward Dipping Reflectors (SDRs) offshore Norway, Greenland, Rockall Plateau, Antarctica, South-west Africa, Northwest Australia, East Coast USA and India (Hinz 1981). SDRs are characterized by their arcuate shape, downdip thickening and offlap patterns, and have generally been attributed to subaerial volcanism associated with Large Igneous Province (LIP) formation prior to the creation of oceanic crust (Planke & Eldholm 1994). Such an origin has been confirmed by the Ocean Drilling

Program (ODP), which has revealed that SDRs comprise numerous lava flows intercalated with volcanoclastic sediments (e.g. Leg 104 (Scientific Party 1987) and Leg 152 (Teagle & Alt 1999)). Refraction data have revealed that SDRs are often associated with high  $P$ -wave velocity lower crustal bodies, which have been interpreted as either a magmatic underplate or sill-like crustal intrusions (White *et al.* 2008). SDRs have been described onshore in Iceland (Bodvarsson & Walker 1964) and in Greenland (Geoffroy *et al.* 1998, 2001), where they are associated with dyke swarms.

Arguably, the best-studied volcanic rifted margins are offshore Norway and Greenland in the North Atlantic Ocean, where their formation has been linked to excess magmatism associated with the Iceland plume (Parkin & White 2008). However, it is not clear whether the flows and intercalated sediments that comprise SDRs are accommodated within the crust by landward dipping border

faults (Gibson & Love 1989; Eldholm *et al.* 1995; Geoffroy *et al.* 2015) or pass vertically into dykes (Mutter *et al.* 1982; Planke & Eldholm 1994; Paton *et al.* 2017) or sills (White *et al.* 2008). As a result, it is not known whether SDRs reflect extensional features, analogous to the fault-bounded sediment filled syn-rift basins that are accommodated within the crust during rifting, or constructional features formed by dyke and sill loading and flexure prior to, during, or following rifting. Part of the difficulty in constraining SDR formation is seismic imaging, which generally does not have the resolution to resolve steeply dipping structures, such as high-angle faults or feeder dykes. Indeed, some reflectors that have been proposed as SDRs in the absence of drilling may not be volcanic, but sedimentary in origin.

It has recently been proposed (Morgan & Watts 2016; Tian & Buck 2016; Buck 2017) that offshore SDRs form by lithospheric flexure in response to dyke and infill loading during the early stages of rifting. In this model, dykes act as a subsurface or buried load, which creates a surface flexure into which subaerial basaltic flows and volcanoclastic sediments accumulate. Since continuous extension allows dykes to be intruded into the crust progressively, the material infilling the surface flexure forms distinct wedge-shape geometries with downdip thickening, resembling the geometries and internal stratigraphy of flexural moats that flank oceanic island and seamount loads in the interiors of oceanic plates.

While Buck (2017) presented examples of seismic reflection profiles of SDRs from rifted margins in the Atlantic and Indian Oceans, he did not quantitatively compare predictions of his flexural model to either seismic or gravity anomaly data. Seismic reflection profile data when depth-migrated provide constraints on the surfaces of flexure and, hence, the long-term strength of extended lithosphere. For example, the widths, thicknesses and internal dips of individual SDR packages can be used to constrain the elastic thickness and how it varies spatially and temporally. The free-air gravity anomaly is sensitive to both the magnitude of the loads and the deformation that they cause. A dyke that intrudes the crust constitutes a mass excess as it cools and solidifies following its emplacement and would be expected to be associated with a positive gravity anomaly; the dyke-driven surface flexure results in a mass deficiency and the displacement of less dense crustal material into denser mantle, and would be expected to be associated with a negative gravity anomaly. The sum gravity anomaly would comprise a central 'high' over the dyke loads which is flanked by 'lows' over the flexure and therefore the SDRs.

The purpose of the paper is to use seismic reflection profiles, together with gravity anomaly data, to constrain the formation SDR packages and their mechanism of emplacement. We focus here on the outer SDR packages that abut oceanic crust, where dyke emplacement appears to be localized. We use a new finite difference model in which dyke loads cause surface flexures that are infilled by volcanoclastic sediment and basaltic lava flows, which is found to be generally in accord with seismic and gravity observations. Furthermore, the model provides constraints on the thermal and mechanical properties, state of stress and long-term strength of extended lithosphere during continental rifting.

## SEISMIC REFLECTION PROFILE DATA

We have compiled a global data set of multichannel seismic reflection profile images and used it to determine the dips of prominent reflectors in offshore SDR packages at volcanic rifted margins as well as their approximate widths and thicknesses (Supporting Information, Table S1; summarized in Table 1). The age of acquisition

of the seismic images (where known) ranges from 1978 to 2015 (Supporting Information Fig. S1). We recognize that acquisition systems have improved significantly during this time. Early systems were based on relatively short analogue streamers and untuned air-gun arrays while more recent systems were based on relatively long (>5 km) digital streamers and tuned arrays. The depth-migrated seismic images acquired by commercial companies, such as ION Geophysical (e.g. Paton *et al.* 2017) have significantly enhanced resolution of Moho, as well as SDRs. The large majority of seismic images in our global database, however, were acquired by academic institutions and have not been depth-migrated. We therefore used the two-way traveltime (TWTT) to convert individual reflectors to depth using a suite of 1-D profiles with assumed velocities between 3 and 5 km s<sup>-1</sup>. Such a range includes the velocities derived from observations such as vertical seismic profiles at ODP boreholes in the feather edge of SDR packages at Site 642 (Planke & Eldholm 1994), sonobuoy data from the South Atlantic (Rabinowitz 1976), and wide-angle seismic refraction data from the Edoras Bank (Barton & White 1997).

As dip is a distinguishing feature of SDRs, we use a moving average of tangential dip measurements along the length of an individual reflector to quantify this. Another difficulty is profile orientation, which may result in measurement of apparent rather than true dip, but this is difficult to correct for in the absence of 3-D seismic data. Fig. 1 shows the method that we use to measure dip on an individual SDR package and a compilation of these dips at the world's volcanic rifted margins. The figure shows measured dips are typically in the range 5°–15°, with few measurements greater than 30°. However, the quality of seismic imaging at the base of SDR packages through basaltic flows and intercalated sediments is poor, and at greater angles is much poorer than at the top of the package, therefore, these greater dips are difficult to accurately constrain.

Other distinguishing features of SDRs are their thickness, width (perpendicular to margin strike) and length (along-strike). Table 1 summarizes our results derived from a representative data set of published seismic reflection profiles over SDRs from major volcanic rifted margins. The majority of SDR packages are between 2- and 6-km-thick, with a mean of 3 km, assuming a *P*-wave velocity range of 3–5 km s<sup>-1</sup>. SDR packages on across-strike margin profiles are typically ~50 km wide, with the narrowest ~15 km (e.g. Rockall, Barton & White 1997) and the widest ~200 km (e.g. Namibia, Koopmann *et al.* 2014). Importantly, we find no correlation between the year of acquisition and measured dip or thickness (Supporting Information Figs S2 and S3), despite significant improvements that have occurred in acquisition as well as processing techniques since the late 1970s.

On some margins, offshore SDR packages are divided into an 'inner' and an 'outer' package, separated by an outer high (e.g. Norway—Planke *et al.* 2000; Namibia—Bauer *et al.* 2000; Argentina—Franke *et al.* 2010). In these cases, the total width may be significantly greater. There are comparatively few along-strike margin profiles of SDRs and so it is difficult to determine their length, but they have been mapped along >2000 km of the East Greenland, and East Coast US rifted margins (Coffin & Eldholm 1994; Planke *et al.* 2000).

## SIMPLE MODEL OF FLEXURE

SDRs are believed to comprise high-extrusion rate lava flows that formed at a subaerial spreading centre, during the early stages of continental rifting (Mutter *et al.* 1982; Planke & Eldholm 1994).

**Table 1.** Condensed compilation of mean values concerning SDR geometry by region.

Region	# Reflectors	Package width (km)	Approx. water depth (km)	Approx. overlying sediment (TWTT/s)	Dip ( $^{\circ}$ )	Std. dev. dip	Thickness (km)	Std. dev. thickness
SW Africa	37	74	2.1	2.0	8	3.7	3.0	0.8
Australia	12	25	3.9	0.6	12	4.5	1.7	0.4
India	14	21	2.1	1.0	16	6.5	2.1	0.7
NE Atlantic	37	34	2.2	0.8	12	5.2	2.7	0.7
S. America	51	60	2.8	2.5	14	5.7	3.6	0.9
GLOBAL	155	53	2.4	1.7	12	5.1	3.0	0.8

See Supporting Information Table S1 for the full data set with individual records per citation. N.B. One profile with four reflectors from the East Coast US was included in the global compilation, but not in this table, due to the small sample size. Approximate water depth and overlying sediment thickness are included as a proxy for amount of stretching. When SDRs are separated into inner and outer packages, the width is measured for each of those packages individually.

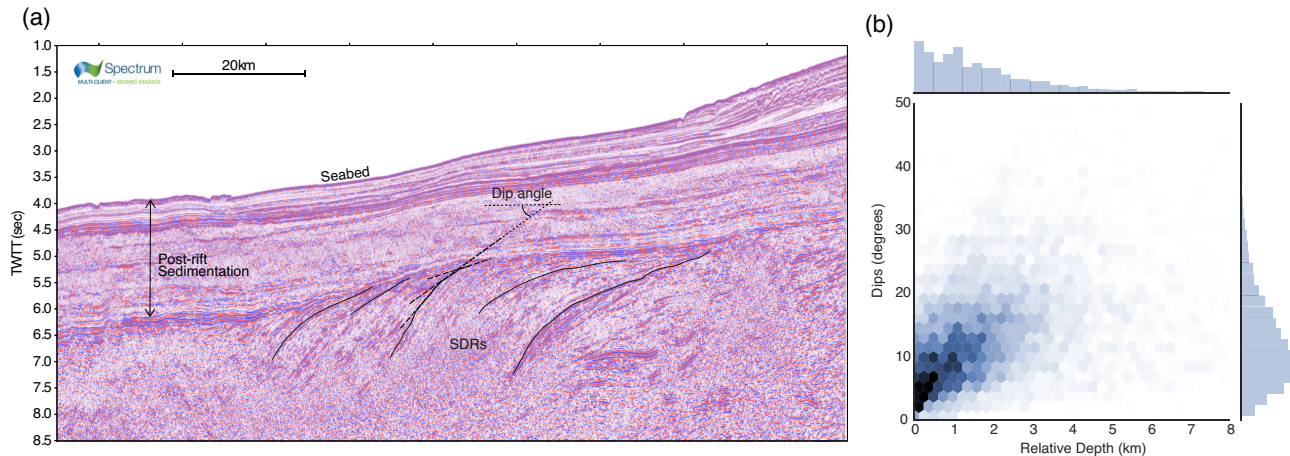


**Figure 1.** (a) Seismic reflection profile offshore southern Namibia in the Orange Basin, provided by Spectrum Geo, location shown in red in Fig. 4(b). Key reflectors within the SDR package are annotated in black. The dashed line tangential to the SDR indicates the method of dip calculation; multiple tangents are taken along the length of the SDR and a moving average calculated. (b) Joint histogram showing global measurements from 155 picked SDRs of dips, and the relative depth of the dip measurement from the top of the SDR package in each case. References and locations of these measurements are given in Supporting Information Table S1, and summarized in Table 1.

The flows are fed by dykes, which are focused at the spreading centre. As extension proceeds, dykes further from the spreading axis are progressively loaded by younger flows, overlapping them and producing a landward dip which is then rotated to form a seaward dip. Such a model does not require faulting and instead creates the accommodation space into which the volcanoclastic sediments and basaltic lava flows accumulate by surface loading.

Similar models have been invoked to explain the stratigraphy of the moats that flank surface volcanic loads at hotspot generated seamount chains. Watts & Cox (1989), for example, modelled the stratigraphy of the Deccan LIP by assuming a volcanic load superimposed on an elastic plate that responded by flexure. The load was assumed to have the approximate dimensions of La Reunion where the plume that generated the flows is believed to be presently located. The ‘Bombay high’ beneath the West Indian shelf and the Chagos-Laccadive Ridge, which links La Reunion to the Deccan lava flows, mark the surface expressions of this load. There is little evidence, however, in the deep seismic structure of volcanic rifted margins for the equivalent surface loads that could have generated SDRs.

Recent approaches to modelling SDR formation have suggested that the arcuate shape of reflectors may also be of flexural origin. Corti *et al.* (2015) showed that downward flexure resulting from a combination of internal (buried) and external (surface) loading can tilt initially horizontal flows toward the injection axis. Paton *et al.*

(2017) sequentially restored SDR packages from an ION Geophysical seismic reflection profile offshore Argentina to demonstrate the progressive rotation of volcanic flows. In their conceptual model, this rotation is driven by a combination of flexural loading due to extrusive igneous material that was fed by sheeted dykes in the upper crust and magmatic intrusions in an overthickened lower crust.

Whereas Paton *et al.* (2017) consider the general state of isostatic balance of oceanic and continental crust, Buck (2017) proposed a model in which subsidence is driven only by dykes which act as intracrustal loads. These subsurface dyke loads intrude the pre-rift crust and cause a surface flexure into which volcanoclastic sediments and basaltic lava flows accumulate, forming SDRs. Buck (2017) used analytical expressions for the flexure of a semi-infinite (i.e. broken) elastic plate overlying an inviscid fluid due to a line load at the plate break to show that surface flexure due to dyke loads could explain the stratigraphic ‘architecture’ of individual SDR packages, in particular their offlap patterns and downdip thickening.

We consider here a similar model to that of Buck (2017). The main difference is that we use a Finite-Difference Method (FDM) of solving the general equation for plate flexure (e.g. Contreras-Reyes & Osses 2010). By using FDM we are able to model distributed rather than single line loads as modelled by Buck (2017). We are also able to consider spatial as well as temporal variations in  $T_e$  during SDR formation, as would be expected to occur, for example,



**Table 2.** Summary of the main parameters assumed in gravity and flexure modelling.

Name	Symbol	Value
Young's modulus	$E$	$1.0 \times 10^{11}$ Pa
Poisson's ratio	$\Sigma$	0.25
Acceleration due to gravity	$G$	$9.8 \text{ m s}^{-2}$
Zero-elevation crustal thickness	-	31.2 km
Density of crust	$\rho_{\text{crust}}$	$2800 \text{ kg m}^{-3}$
Density of upper mantle	$\rho_{\text{mantle}}$	$3330 \text{ kg m}^{-3}$
Density of load	$\rho_{\text{load}}$	$2950 \text{ kg m}^{-3}$
Density of volcanoclastic infill	$\rho_{\text{infill}}$	$2700 \text{ kg m}^{-3}$
Dyke height	$h$	-
Dyke width	$w$	-
Elastic thickness	$T_e$	-

from numerical models of the dynamics of rifting (Burov & Poliakov 2001). Finally, we consider both infinite and semi-infinite (i.e. broken) plate flexure. In the latter case, the plate break is simulated by  $T_e = 0$  at the point of intrusion.

Our model comprises two main stages. In the first stage, a dyke with a specified height, width and density,  $\rho_{\text{load}}$ , is emplaced at the axis of spreading, with the dyke's flat top set at zero depth. We assume that the dyke is the load which drives the initial flexure. The initial flexure is calculated assuming an air infill (i.e.  $\rho_{\text{infill}} = 0$ ) in accord with the observations in ODP site 642 (Planke & Eldholm 1994) and DSDP sites 342 (Scientific Party 1976) and 553 (Scientific Party 1984) of cores with subaerial, weathered flow tops in SDR packages. In the second stage, the initial flexure is infilled to the assumed horizontal pre-deformation surface by volcanoclastic sediments and basaltic lava flows, (i.e.  $\rho_{\text{infill}} \neq 0$ ) which drives further flexure. The total subsidence for this combined dyke and infill load represents a single SDR flow unit. After calculating the flexure, the crust is extended by splitting the model at the spreading axis and intruding the next dyke load, which will drive further flexure and form a second SDR flow unit.

We assume that the material infilling the flexure is of uniform density at each time step. The infill in the region of the subsidence will differ, however, from the infill of the uplift regions; this is difficult to model without iterating for the flexure at each stage as it is dependent on the elastic thickness. In the first dyke-driven stage, the infill used in the subsidence (air) is the same as in the uplift regions and therefore our assumption is valid. However, in the second stage where volcanoclastic infill is used, this is no longer true, subduing the flexural bulge and increasing the width of the SDR package. Alternatively, we may use non-zero infill values in the subsided areas at the infill driven stage, and use the density of air in all other regions. In this case, we underestimate the overall infilling density and therefore the size of the package as the total subsidence is wider than the initial load driven subsidence. The difference between these two end member cases for the typical model inputs is, however, small (Supporting Information Fig. S4).

The least well-constrained input parameter in our model is the dyke height, which is a major control on the thickness of the SDR package. The total thickness is determined by the height and width of the load, the densities of infill,  $\rho_{\text{infill}}$ , substrate,  $\rho_{\text{mantle}}$ , dyke load,  $\rho_{\text{load}}$  and host rock,  $\rho_{\text{crust}}$  and  $T_e$ . As densities can be prescribed within plausible ranges (Table 2) and  $T_e$  is constrained by the width of the package, we can use the observed thickness of the SDR package to inform the choice of dyke height. We assume here 15 km for the dyke height, which is of the order of the seismogenic layer thickness and vertical extent of faulting and earthquakes in

continental rifts (Ebinger 2005) and produces SDR packages of reasonable thicknesses.

In a rifted, thermally subsiding, margin setting subaerial SDR packages will eventually be driven below sea-level, and because extension varies laterally, they may be rotated. We have therefore superimposed the modelled SDR package that forms following dyke loading onto a rifted margin profile, calculated assuming uniform stretching, finite rifting and lateral heat flow (Cochran 1983). For modelled narrow margins, this process adds a few degrees of rotation to the dips of the SDRs. The final SDR stratigraphy after thermal subsidence was then analysed using the same moving average dip calculation as was used on the global seismic reflection data (Fig. 1).

We found that the overall stratigraphy of a SDR package depends on the type of flexure model used and the  $T_e$  assumed. The arcuate shape of SDRs can only be produced by using a broken plate model, or continuous plate model which is significantly weaker at the point of dyke injection. This weakening may, of course, be the cause of dyke localization, before the initiation of seafloor spreading.

Using a numerical approach to the calculation of flexure for each load allows consideration of the lateral variation of  $T_e$ . The model accepts three arguments—the maximum  $T_e$ , minimum  $T_e$  and a distance over which a linear gradient between these two values should be implemented from the position of dyke intrusion outwards. The default value for this distance is the half-width of the dyke, such that the zone of weakness is the total width of the dyke. Increasing the width of this zone of weakness results in changes to the stratigraphy of the package; in general, a wider weak zone relative to the dyke width results in greater downdip thickening and more pronounced increases in dip as depth increases. This results from the localization of the subsidence associated with each dyke in a narrower zone compared to a plate with a more uniform  $T_e$ .

As subsequent SDR flow units form, our model implies that there should be some rotation of the feeder dykes, increasing with distance from the spreading axis, as shown by the red coloured markers of the dyke tops in Fig. 2. However, thin elastic plate theory as we have assumed here only produces vertical flexures, so the deflection of an initially vertical surface cannot be accurately modelled. We have therefore shown the dykes as vertical in Fig. 2, although we recognize that some rotation and internal deformation may occur as SDR packages evolve and the margin subsides. Nearly vertical and inclined reflections attributed to SDR feeder dykes have been identified in seismic reflection data from the Vøring margin (Abdelmalak *et al.* 2015). In onshore field analogues, Abdelmalak *et al.* (2015) identify multiple generations of cross-cutting feeder dykes which have been progressively rotated, consistent with a flexural model.

As demonstrated by Buck (2017) in his analytical modelling, the dyke loading model can be extended to shifts in the loci of intrusion, as occurs, for example, during a ridge jump in mature mid-ocean ridge settings. These jumps will produce asymmetry on the eventual conjugate margins, in both thickness and dip of an SDR package. Supporting Information Fig. S5 shows that in the case of a ridge jump our numerical models produce similar geometries to those described by Buck (2017).

## ISOSTATIC GRAVITY ANOMALIES

A critical test of the validity of all flexure models is the gravity anomaly, since it is sensitive to both the driving loads and the resulting flexures. We have shown that a flexure model of dyke

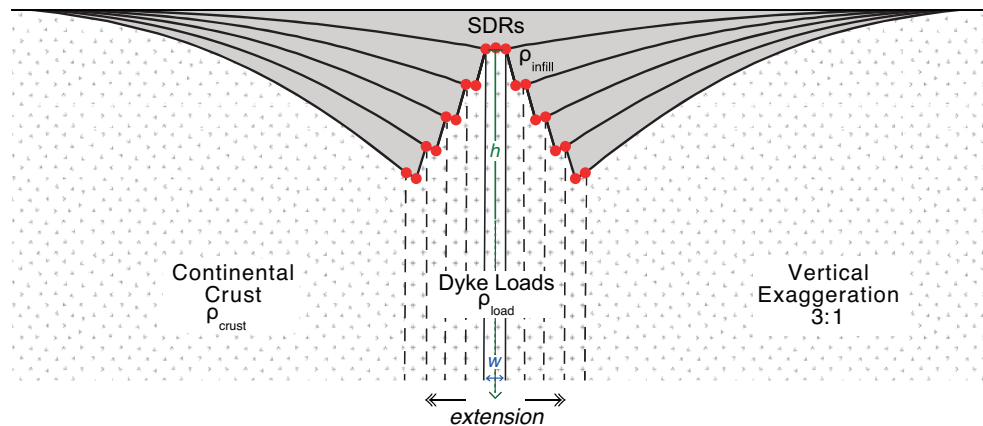


**Figure 2.** Simple model of flexure for the formation of SDRs in volcanic rifted margins. Subsurface dyke loads intrude the crust and cause a surface flexure that is subsequently infilled by volcanoclastic and basaltic lava flows (shaded grey). The red circles show the tilting of the dyke tops that occurs as a result of progressive dyke loading and associated flexure, with the vertical dyke boundaries shown in dashed lines. The dyke tops are rotated as flexure progresses, such that the sides of the dykes may also be rotated. However, this cannot be accurately resolved within our thin elastic plate model.

and infill loading can predict geometries that match those of SDRs observed on seismic reflection data, both in terms of overall width and thickness and stratigraphic dip. However, the internal velocity structure and consequently the thickness of SDRs is generally not well constrained from seismic data, so it is useful to use the gravity anomaly as an additional constraint on models for SDR formation.

In order to calculate the gravity effect of SDRs, we take a Process-Oriented Gravity Modelling (POGM) approach, similar to that used by Watts (1988) to calculate the contributions of rifting, sedimentation and erosion to the free-air gravity ‘edge effect’ anomaly at the non-volcanic Baltimore Canyon Trough, East Coast USA rifted margin. This approach has also been used to calculate the contribution of magmatic underplating to the ‘edge effect’ anomaly at the British Isles rifted margin (Watts & Fairhead 1997). Here, we extend the POGM methodology to include the gravity effect of subsurface intrusive dyke loads and their associated extrusive infill loads, isolating in the process the so-called dyke and SDR gravity anomalies. These anomalies can then be summed and compared to observed gravity anomalies.

We assume, following Mutter *et al.* (1982), that SDRs originate at sea-level and then subside following rifting, cooling and thermal contraction. There will therefore be a rifting gravity anomaly in addition to a dyke and SDR anomaly. The rifting anomaly depends on the mode of extension and is given by the combined gravity effect of the water-filled tectonic subsidence and the isostatically balanced Moho uplift. The dyke anomaly subdivides into three main contributions: a gravity high associated with the dyke load and flanking gravity lows associated with the load-driven flexure at both the top and base of the crust. The SDR anomaly subdivides similarly: a gravity high associated with the lava and volcanoclastic material infilling the pre-existing, air-filled subsidence and flanking lows associated with the additional flexure at the top and base of the crust. All anomalies can be computed from the implied mass distributions using a line-integral method (e.g. Bott 1960) and the attenuating effects of the increase in water depth that follows rifting can be included in the dyke and SDR anomaly calculation.

Fig. 3 shows the dyke and SDR anomaly, together with the sum anomaly which reflects the gravity effect of all the magmatic processes to have modified the margin since rifting. The dyke and SDR anomalies (Figs 3a and b) comprises a high flanked by lows that reflects the mass excess of the loads and the mass deficiency of

the associated flexures. The sum anomaly (Fig. 3c) also comprises a high flanked by lows with the high delineating the extent of the dyke loads and the lows the extent of the SDRs. The sum anomaly increases in amplitude and wavelength with increase in  $T_e$ . Irrespective of  $T_e$ , the model predicts that the maximum gradient of the sum anomaly corresponds to the contact between the dyke load and the SDRs.

The sum anomalies in Fig. 3 do not include the rifting anomaly and so they can be compared directly to observed Airy isostatic gravity anomalies. This is because the Airy isostatic gravity anomaly is the free-air anomaly *less* the gravity effect of the topography and its Airy-type compensation and so the anomaly already includes a correction for the thinning of the crust that results from rifting.

We have derived the observed Airy isostatic gravity anomaly from the  $1 \times 1$  min free air gravity anomaly grid (Version 23.1) of Sandwell *et al.* (2014) and the  $1 \times 1$  min GEBCO bathymetry grid of B.O.D.C. (2014), assuming a zero-elevation crustal thickness of 31.2 km and an average crustal density of  $2800 \text{ kg m}^{-3}$ . Spherical harmonics from degree and order 2–20 (EGM 2008, Pavlis *et al.* 2012) have been removed from the anomaly in order to remove long wavelength effects associated, for example, with dense subducted slabs. We have not corrected the observed Airy isostatic gravity anomaly for the effect of the post-rift sediments and their compensation. However, these sediments have accumulated over an area of the continental slope and rise that is much larger than individual SDR packages and so their gravity effect will be significantly longer in wavelength than the contributions associated with magmatism.

## CASE STUDY: THE NAMIBIA RIFTED MARGIN

We have applied our model of SDR formation to the Namibia volcanic rifted margin (Fig. 4). This margin was selected because Spectrum Geo provided us access to a closely spaced ( $\sim 5$ – $10$  km) seismic reflection profile data set on which SDRs can be easily identified and their dips measured (e.g. Fig. 1).

The model parameters that best fit the geometry of the offshore Namibia SDRs are  $T_e$  in the range 1.25–3 km, a dyke height of 15 km and a total dyke intrusion width of 75 km. The maximum thickness of the modelled package of 5 km is also consistent with

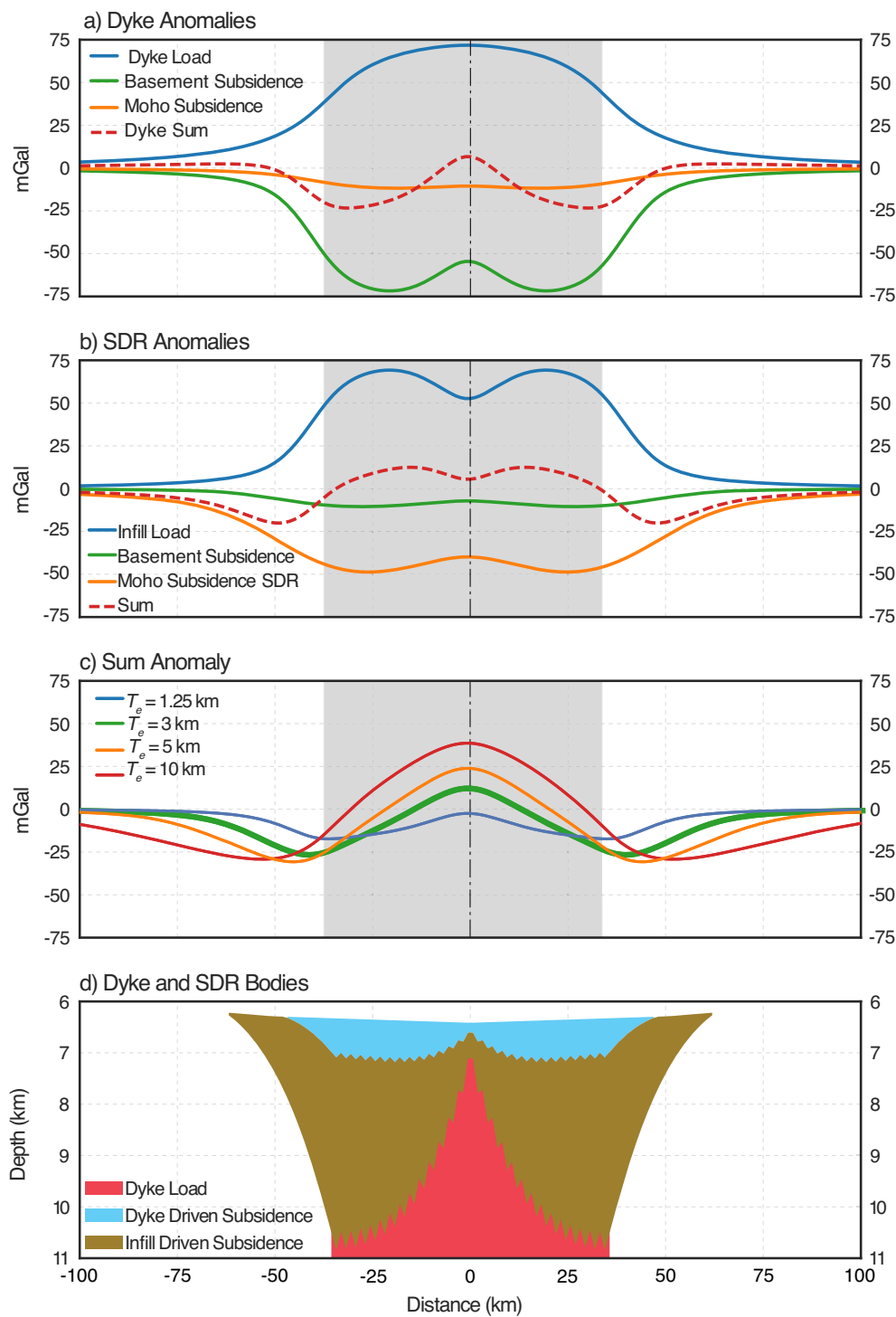


**Figure 3.** POGM of SDR formation using values from Table 2 with a dyke height of 15 km and a  $T_e$  of 3 km. (a) Dyke gravity anomaly. (b) SDR gravity anomaly. (c) Sum gravity anomaly (a + b) with  $T_e = 3$  km shown in the thick line, other  $T_e$  values (all other parameters equal) shown for comparison. (d) Dyke and SDR bodies. Red shade = dyke load. Blue shade = dyke driven subsidence and subsequent infill load. Green shade = infill driven flexure. The final SDR package will incorporate both the blue and brown regions. Vertical dashed line in panels (a)–(c) delineates the location of future continental rifting and break-up; grey shaded rectangle indicates the lateral extent of dyking.

observations, assuming the internal velocity of the package is in the range 3–5 km s<sup>-1</sup>.

The SDR package produced by the best-fit model and the dips associated with this are shown in Fig. 5. We find dip values here are very close to the global average, typically in the range 5°–15°.

The observed dips were derived from the Spectrum Geo seismic reflection data shown in Fig. 1. The calculated dips were derived from the best-fit model output using the same method as was used in the observed seismic data. There is a good general agreement between the two data sets, both of which show increasing dip with



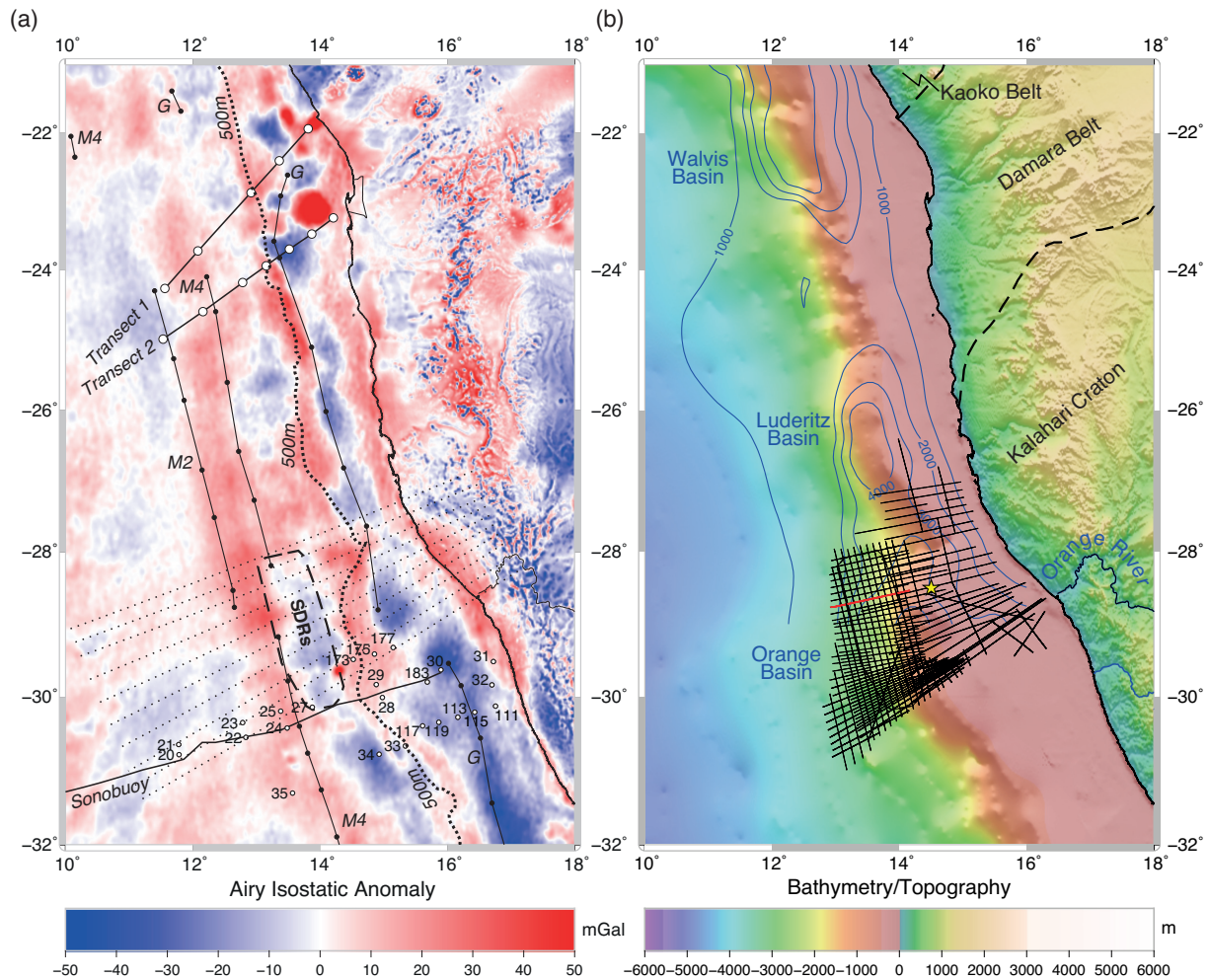


**Figure 4.** Airy isostatic gravity anomaly and bathymetry of the volcanic rifted margin offshore Namibia. The extent of the SDR package identified from the seismic reflection data is shown by the polygon with dashed black line. (a) Airy isostatic gravity anomaly with the degree and order 20 gravity field removed. Heavy dotted black line shows the 500 m isobath. Thin solid lines with filled black circles show magnetic lineations M2 (~124 Ma) and M4 (~127 Ma) and the 'G' anomaly or 'LMA' (Rabinowitz & Labrecque 1979; Moulin *et al.* 2010; Collier *et al.* 2017). Thick solid line with associated white circles and numbers show the Sonobuoy profile of Rabinowitz (1976). Transects 1 and 2 show the seismic refraction profiles of Bauer *et al.* (2000). Light dotted black lines indicate the location of the profiles used to calculate the ensemble average shown in Fig. 5(c). (b) Bathymetry. Thin solid black lines show the location of available Spectrum Geo seismic reflection survey; red line is the profile shown in Fig. 1. Contours at 1000 m interval in blue show the total post-rift (Aptian to present) sediment thickness from Stewart *et al.* (2000). Yellow star indicates the location of the Kudu 9A-1 well. Key geological features also labelled, from Bauer *et al.* (2000).

depth beneath the top of the SDR package. The most common values of dip are similar ( $\sim 5^\circ$ ) and occur at shallow depths. The main discrepancies are for high dips and deep depths. The calculated dip versus depth plot flattens with depth while the observed dip versus depth continues to increase. This is probably the consequence of uncertain velocities near the base of observed SDR packages. In order to quantify the best-fit  $T_e$  in terms of the resulting dip distribution, we calculate the cosine similarity between the normalized, binned data sets shown in the histogram (Fig. 5b). We find a best-fit  $T_e$  in the range 2–3 km, as shown in Fig. 6.

The calculated gravity anomaly also fits observations (Fig. 5c), matching the Airy isostatic gravity anomaly gradient at the landward edge of the SDRs reasonably well. Quantifying the fit to the observed isostatic anomaly using a root-mean squared error, the best-fit  $T_e$  is 1.25 km (Fig. 6). This fits the gradient over the dyke-SDR contact very well, but the width of the package is better fit by a slightly higher  $T_e$ , in the range 3–5 km. This produces a larger

amplitude gravity anomaly, within the range of the observed profiles shown in Fig. 5(c), but larger than the ensemble average.

These  $T_e$  values are small; however, Buck (1988) and Roberts *et al.* (1993) have used similar small values in order to constrain the geometry of faulting and syn-rift basins during the initial stages of continental break-up. The  $T_e$  values imply curvatures of up to  $10^{-5} \text{ m}^{-1}$  which, depending on the crust and upper mantle rheology, suggest significant yielding (<60–70%) of the flexed plate and a reduction in thickness as the plate thins from its short-term mechanical thickness to its long-term elastic thickness.

Unusually for a volcanic rifted margin, a second gravity anomaly high is present offshore Namibia, inboard of the isostatic gradient coincident with the M4 magnetic anomaly. The landward gradient of this high correlates with the 'G' magnetic anomaly. This has previously been modelled as an edge effect associated with the Ocean/Continent boundary (Talwani & Eldholm 1973; Rabinowitz 1976). Moulin *et al.* (2010) redefined the 'G' anomaly,

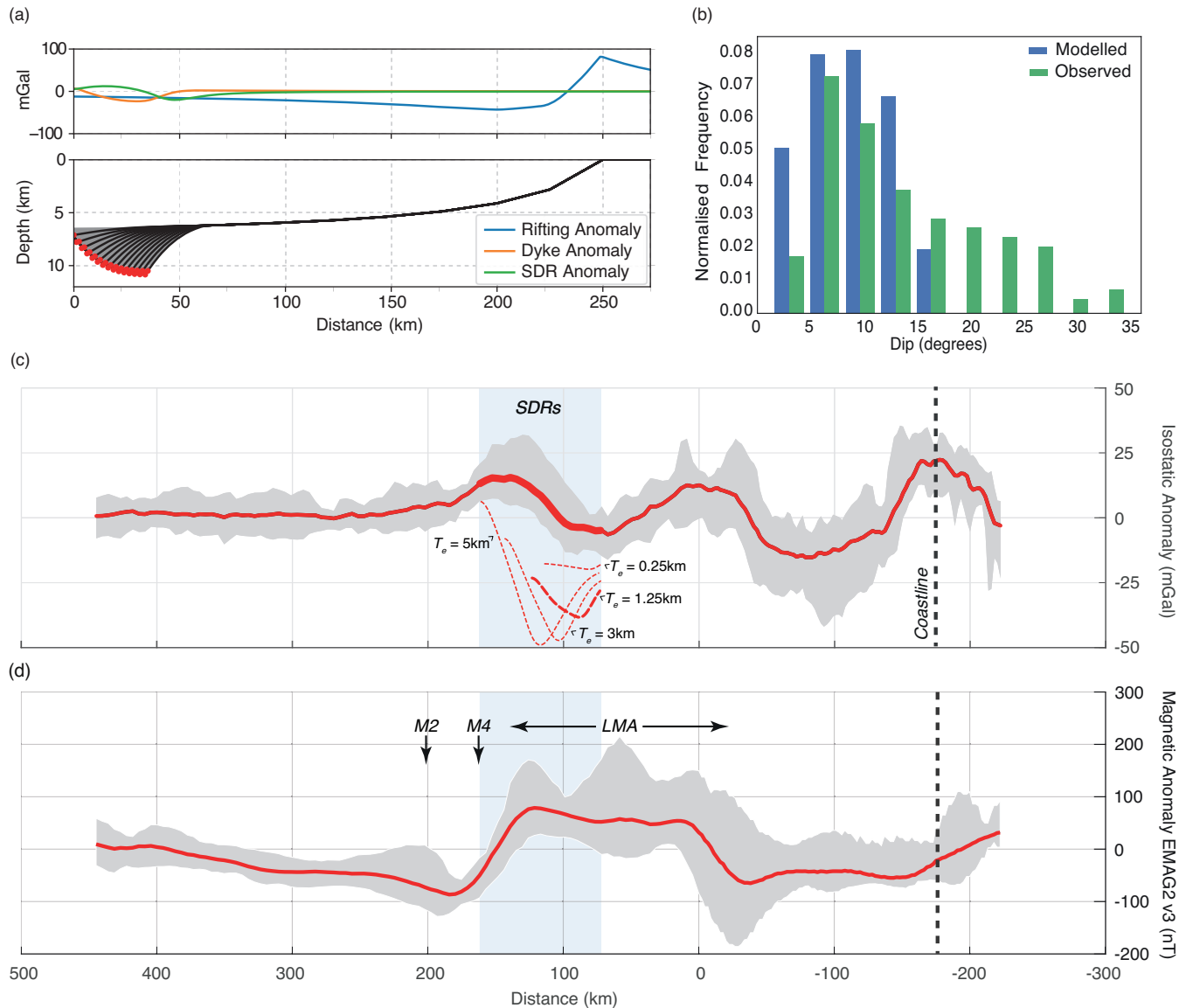


**Figure 5.** (a) Post-rift model stratigraphy and components of gravity anomaly for  $T_e = 3$  km; the rifting anomaly is shown in blue, indicating that the ‘edge effect’ lies far from the SDRs. The rifting anomaly was calculated from the gravity effect of the water-filled tectonic subsidence and the compensating oceanward thinning of the continental crust, assuming a uniform stretching model and Airy isostasy. The calculated Dyke and SDR anomalies shown are from Fig. 3 that incorporate the water depth. (b) Normalized histogram of observed versus modelled dips for a  $T_e$  of 3 km. (c) Ensemble average (red) of observed Airy Isostatic Anomaly profiles (range shown in grey) shown in Fig. 4. The blue shaded vertical bar indicates the region in which SDRs have been located on seismic reflection data; the dashed black line indicates the intersection with the coastline. The dashed red lines show the modelled result (offset vertically for comparison) for  $T_e$  of 0.25, 1.25, 3 and 5 km, with best-fit 1.25 km in bold. These curves are shown only for the region in the model that corresponds with the extent of the SDRs and are positioned such that the well-constrained landward edge of the SDR package matches the observed. (d) Corresponding ensemble average of the observed magnetic anomaly (EMAG2 v3, Meyer *et al.* 2017). ‘LMA’, ‘M4’ and ‘M2’ indicate the location of the magnetic anomalies (Rabinowitz 1976; Moulin *et al.* 2010). The seaward gradient of the ‘LMA’ has been interpreted by Collier *et al.* (2017) as the seaward limit of the outer SDRs, consistent with our seismic and gravity anomaly observations.

when grouped with the M11 and M9 anomalies of Rabinowitz & Labrecque (1979), as the Large Marginal Anomaly (LMA). The LMA (Fig. 5d) is characterized by a large amplitude and irregular width signature (Moulin *et al.* 2010), unlike linear seafloor spreading anomalies, and corresponds well with SDRs mapped in seismic studies of in the Walvis Basin (Bauer *et al.* 2000; Koopmann *et al.* 2014).

Magnetic modelling of SDR packages in the South Atlantic by Collier *et al.* 2017 demonstrated that the inner SDRs, which lie above transitional continental crust, would not be associated with

detectable linear anomalies. In contrast, the outer SDRs, underlain by igneous crust composed of continuous dykes, as we propose here, are associated with linear magnetic anomalies. We find a second, landward package of subhorizontal, dipping reflectors in the Orange Basin, but this package does not correspond with a gradient in isostatic anomaly, as expected within our proposed flexural model. Nor does the package show the typical arcuate downdip thickening of reflectors characteristic of outer SDRs. This supports an alternative origin for the inner SDRs, likely developed at an earlier stage of rifting, which may be fault controlled.



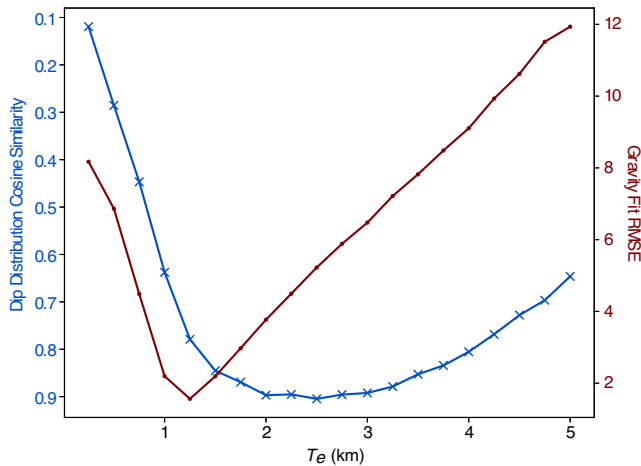


**Figure 6.** Measure of best-fit for different  $T_e$  values to observed gravity anomaly (red circles, root-mean squared error) and dip distribution (blue crosses, cosine similarity) in Orange Basin, Namibia. The cosine similarity is calculated from normalized vectors of binned dip measurements.

## DISCUSSION

We have assumed that the architecture of SDRs reflects magmatic processes that have modified the margin since the initiation of extension. Further, we assume that only an initial mechanical subsidence followed by a gentle thermal subsidence have modified them subsequent to formation. Therefore, we have ignored the possible contributing effects of post-rift sedimentation, faulting and inversion to the present-day dips of SDRs. We point out, however, that we have been able to explain the observations without invoking other processes suggesting that the combined effects of these other factors on SDR geometry are small. Therefore, a relatively simple model of dyke-driven flexure in combination with an initial and thermal subsidence can explain the observations and this is despite the fact that the initial flow of basalt during SDR formation may have been in a *landward* direction, away from the axis of the future rift.

### SDR reflectivity

An outstanding question is whether our models for SDR formation are compatible with the internal structure and reflectivity of an individual SDR package. In order to address this question, we have used a convolutional method (Yilmaz 2001) to ray trace model outputs and construct a preliminary set of synthetic zero-offset Common Depth Point gathers that can be compared to observed reflection profiles. We assumed a velocity/density model in which the dyke-driven infill comprises volcanoclastic sediment with intercalated lava flows, by alternating the infill value ( $2600\text{--}2700\text{ kg m}^{-3}$ ) between dykes. We found that such a layered sequence, as shown in Supporting Information Fig. S6, which is compatible with direct sampling data (Teagle & Alt 1999), is necessary within the infill to provide the impedance contrast required. We also found that the dyke loads that generate the infill will not be imaged due to their steep, near vertical, contact with the surrounding crust. If there is no significant variability in the density of the intruding dykes through time, there will also be a lack of density/velocity contrasts to image within the dyke body.

### Isostatic gravity anomalies

The Airy isostatic gravity anomaly is a useful parameter with which to examine the structure of rifted margins. Talwani & Eldholm (1973), for example, used the landward gradient of a prominent Airy isostatic anomaly high to locate a change in basement age and depth which they attributed to the ocean/continent boundary. Other explanations of the high include flexure due to sediment loading (Karner & Watts 1982). In this paper, we have interpreted the landward gradient of the high as marking the boundary of the seaward limit of the SDR package at the contact between the low density (compared to crustal rocks) infill material and the high-density dykes. The landward gradient does not, therefore, correspond to the Ocean/Continent boundary *per se* but, lies somewhat landward of it and marks the transition from ‘magmatic’ intruded stretched continental crust with associated SDRs to true continental crust.

### Flexure and the role of faulting

We have assumed thus far a model in which outer SDRs that abut oceanic crust form by dyke-driven loading and associated flexure. Listric faults and landward dipping detachments (e.g. Gibson & Love 1989; Eldholm *et al.* 1995; Geoffroy *et al.* 2015) which could help accommodate SDRs within the brittle upper crust are not required in order to explain the seismic and gravity observations. Some form of faulting may, however, accompany SDR formation as is evidenced by the high plate curvatures (up to  $\sim 10^{-5}\text{ m}^{-1}$ ) which would normally be indicative of significant yielding of the plate.

We note that at volcanic rifted margins with distinct sets of inner and outer SDRs, it has been proposed that they form by different mechanisms active during different stages of rifting. Outer SDRs form by loading and flexure, as modelled here, while inner SDRs may be fault controlled (Barton & White 1997; Planke *et al.* 2000). We do not know if the inner and outer SDRs at these margins are contemporaneous. One possibility is that inner SDRs are older than outer SDRs and reflect brittle deformation in the shallow crust, while outer SDRs reflect flexure of a weakened lithosphere with an elastic ‘core’ that has been thinned by both brittle and ductile deformation.

### Long-term strength of extended continental lithosphere

We know from numerical geodynamic modelling (Burov & Poliakov 2001) that rifting changes the integrated strength of the lithosphere: weakening it during the syn-rift and strengthening it during the early post-rift. SDR formation could occur during either or both of these contrasting strength regimes. We found that decreasing  $T_e$  for each dyke as loading progresses produces offlap at the edges of an SDR package and a flattening of its base (Fig. 7b). This tendency to offlap could produce long ‘trains’ of near horizontal SDRs with no single pinch out point, or flexural node, as is frequently observed. This is consistent with the pre-existing crust in the region of intrusion weakening as rifting progresses. In contrast, we found that increasing  $T_e$  for successive dyke loads results in onlap at the edges of a SDR package and a marked relief at its base (Fig. 7a). However, onlap is not typically observed in SDR packages, suggesting they are emplaced during the early weakening phase rather than during the later strengthening phase of rift margin evolution.

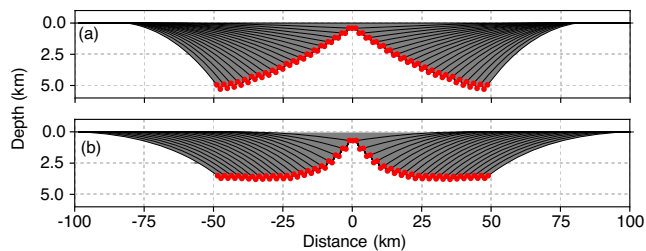


**Figure 7.** (a) Increasing  $T_e$  and (b) decreasing  $T_e$  with successive loads resulting in onlap and offlap, respectively. Parameters used are shown in Table 2, with a dyke height of 15 km. In both cases, the total width of dyking is 100 km, with the  $T_e$  varying between 3 and 6 km.

## CONCLUSIONS

We draw the following conclusions from this study:

- (1) Offshore SDRs can be explained by a simple model of flexure in which subsurface dyke loads create surface flexures that are subsequently infilled by volcanoclastic and basaltic lava flows.
- (2) Flexure models generally account for the width, thickness and downdip thickening of SDR packages as revealed in seismic reflection profile data over volcanic rifted margins.
- (3) A flexural origin for outer SDRs is supported by isostatic gravity anomaly 'highs' and flanking 'lows' which reflect the dyke and infill loads and resulting flexures respectively.
- (4) The flexure parameters that best fit seismic and gravity anomaly data suggest either a broken plate or a continuous plate that has been significantly weakened at the point of intrusion, and is associated with relatively low values of elastic thicknesses (1–3 km) with yielding.
- (5) The lack of onlap at the landward edges of SDRs suggests that they are emplaced when the long-term strength of the lithosphere is progressively weakening.

## ACKNOWLEDGEMENTS

We thank Roger Buck and Xiaochuan Tian for discussions and for hosting RLM during a recent visit to Lamont-Doherty, Spectrum Geo for provision of seismic reflection profile data and Joe Cartwright (Oxford) for discussions. We thank Jenny Collier and two anonymous reviewers for their comments, which improved earlier versions of this manuscript. This work was supported by the Natural Environment Research Council NE/L002612/1 and RCUK/St John's College scholarship to RLM and NERC NE/1026839/1 to ABW.

## REFERENCES

Abdelmalak, M.M. *et al.*, 2015. The ocean-continent transition in the mid-Norwegian margin: insight from seismic data and an onshore Caledonian field analogue, *Geology*, **43**, 1011–1014.  
 B.O.D.C., 2014. *General bathymetric Chart of the Oceans (GEBCO)*. [http://www.gebco.net/data\\_and\\_products/gridded\\_bathymetry\\_data/](http://www.gebco.net/data_and_products/gridded_bathymetry_data/).  
 Barton, A.J. & White, R.S., 1997. Volcanism on the Rockall continental margin, *J. geol. Soc.*, **154**, 531–536.  
 Bauer, K. *et al.*, 2000. Deep structure of the Namibia continental margin as derived from integrated geophysical studies, *J. geophys. Res.*, **105**, 25829–25853.  
 Bodvarsson, G. & Walker, G.P.L., 1964. Crustal drift in Iceland, *Geophys. J. R. astr. Soc.*, **8**, 285–300.

Bott, M.H.P., 1960. The use of rapid digital computing methods for direct gravity interpretation of sedimentary basins, *Geophys. J. R. astr. Soc.*, **3**, 63–67.  
 Buck, W.R., 1988. Flexural rotation of normal faults, *Tectonics*, **7**, 959–973.  
 Buck, W.R., 2017. The role of magmatic loads and rift jumps in generating seaward dipping reflectors on volcanic rifted margins, *Earth planet. Sci. Lett.*, **466**, 62–69.  
 Burov, E. & Poliakov, A., 2001. Erosion and rheology controls on synrift and postrift evolution: verifying old and new ideas using a fully coupled numerical model, *J. geophys. Res.*, **106**, 16 461–16 481.  
 Cochran, J.R., 1983. Effects of finite extension times on the development of sedimentary basins, *Earth planet. Sci. Lett.*, **66**, 289–302.  
 Coffin, M.F. & Eldholm, O., 1994. Large igneous provinces: Crustal structure, dimensions, and external consequences, *Rev. Geophys.*, **32**, 1–36.  
 Collier, J.S., McDermott, C., Warner, G., Gyori, N., Schnabel, M., McDermott, K. & Horn, B.W., 2017. New constraints on the age and style of continental breakup in the South Atlantic from magnetic anomaly data, *Earth planet. Sci. Lett.*, **477**, 27–40.  
 Contreras-Reyes, E. & Osses, A., 2010. Lithospheric flexure modelling seaward of the Chile trench: implications for oceanic plate weakening in the trench outer rise region, *Geophys. J. Int.*, **182**, 97–112.  
 Corti, G., Agostini, A., Keir, D., van Wijk, J., Bastow, I.D. & Ranalli, G., 2015. Magma-induced axial subsidence during final-stage rifting: implications for the development of seaward-dipping reflectors, *Geosphere*, **11**, 563–571.  
 Ebinger, C.J., 2005. Continental break-up: the East African perspective, *Astron. Geophys.*, **46**, 2.16–12.21.  
 Eldholm, O., Skogseid, J., Planke, S. & Gladczenko, T.P., 1995. Volcanic margin concepts, in: *Rifted Ocean-Continent Boundaries*, pp. 1–16, eds Banda, E., Torné, M. & Talwani, M., Kluwer Academic Publishers, Dordrecht.  
 Franke, D., Ladage, S., Schnabel, M., Schreckenberger, B., Reichert, C., Hinz, K., Paterlini, M., de Abelleira, J. & Siciliano, M., 2010. Birth of a volcanic margin off Argentina, South Atlantic, *Geochem. Geophys. Geosyst.*, **11**(2).  
 Geoffroy, L., Burov, E.B. & Werner, P., 2015. Volcanic passive margins: another way to break up continents, *Nat. Sci. Rep.*, **5**, 1–12.  
 Geoffroy, L., Gelard, J.P., Lepvrier, C. & Olivier, P., 1998. The coastal flexure of Disko (West Greenland), onshore expression of the 'oblique reflectors', *J. geol. Soc.*, **155**, 463–473.  
 Geoffroy, L. *et al.*, 2001. Southeast Baffin volcanic margin and the North American-Greenland plate separation, *Tectonics*, **20**, 566–584.  
 Gibson, I.L. & Love, D., 1989. A listric fault model for the formation of the dipping reflectors penetrated during the drilling of hole 642E, ODP leg 104, in: Eldholm, O., Thiede, J. & Taylor, E., *et al.*, *Proc. ODP, Scientific Results*, **104**, College Station, TX (Ocean Drilling Program), 979–983.  
 Hinz, K., 1981. A hypothesis on terrestrial catastrophes: wedges of very thick oceanward dipping layers beneath passive margins—their origin and paleoenvironment significance, *Geol. Jahrb.*, **E22**, 345–363.  
 Karner, G.D. & Watts, A.B., 1982. On isostasy at Atlantic-type continental margins, *J. geophys. Res.*, **87**, 2923–2948.  
 Koopmann, H., Franke, D., Schreckenberger, B., Schulz, H., Hartwig, H., Stollhofen, H. & di Primio, R., 2014. Segmentation and volcano-tectonic characteristics along the SW African continental margin, South Atlantic, as derived from multichannel seismic and potential field data, *Mar. Pet. Geol.*, **50**, 22–39.  
 Meyer, B., Saltus, R. & Chulliat, A., 2017. *EMAG2: Earth Magnetic Anomaly Grid (2-arc-minute resolution) Version 3*, National Centers for Environmental Information, NOAA. Model.  
 Morgan, R.L. & Watts, A.B., 2016. *Isostatic Gravity Anomalies, Flexure and the Origin of Seaward Dipping Reflectors at Volcanic Rifted Margins 2016 Fall AGU Meeting*, EOS.  
 Moulin, M., Aslanian, D. & Unternehr, P., 2010. A new starting point for the South and Equatorial Atlantic Ocean, *Earth Sci. Rev.*, **98**, 1–37.  
 Mutter, J.C., Talwani, M. & Stoffa, P.L., 1982. Origin of seaward-dipping reflectors in oceanic crust off the Norwegian Margin by "subaerial seafloor spreading", *Geology*, **10**, 353–357.

- Parkin, C.J. & White, R.S., 2008. Influence of the Iceland mantle plume on oceanic crust generation in the North Atlantic, *Geophys. J. Int.*, **173**, 168–188.
- Paton, D.A., Pindell, J., McDermott, K., Bellingham, P. & Horn, B., 2017. Evolution of seaward-dipping reflectors at the onset of oceanic crust formation at volcanic passive margins: insights from the South Atlantic, *Geology*, **5**, 439–442.
- Pavlis, N.K., Holmes, S.A., Kenyon, S.C. & Factor, J.K., 2012. The development and evaluation of the Earth gravitational model 2008 (EGM2008), *J. geophys. Res.*, **117**.
- Planke, S. & Eldholm, O., 1994. Seismic response and construction of seaward dipping wedges of flood basalts: Voring volcanic margin, *J. geophys. Res.*, **99**, 9263–9278.
- Planke, S., Symonds, P.A., Alvestad, E. & Skogseid, J., 2000. Seismic volcanostratigraphy of large-volume basaltic extrusive complexes on rifted margins, *J. geophys. Res.*, **105**, 19335–19351.
- Rabinowitz, P.D., 1976. Geophysical study of the continental margin of southern Africa, *Bull. geol. Soc. Am.*, **87**, 1643–1653.
- Rabinowitz, P.D. & LaBrecque, J., 1979. The Mesozoic South Atlantic Ocean and evolution of its continental margins, *J. geophys. Res.*, **84**(B11), 5973–6002.
- Roberts, A.M., Yielding, G., Kusznir, N.J. & Dorn-Lopez, D., 1993. Mesozoic extension in the North Sea: constraints from flexural backstripping, forward modelling and fault populations, in *The Petroleum Geology of Northwest Europe*, pp. 1123–1136, eds Parker, J.R., Geological Society of London.
- Sandwell, D.T., Müller, R.D., Smith, W.H.F., Garcia, E. & Francis, R., 2014. New global marine gravity model from CryoSat-2 and Jason-1 reveals buried tectonic structure, *Science*, **346**, 65–67.
- Scientific Party, 1976. Sites 338–343, in *Initial Reports, DSDP*, pp. 151–387, eds Talwani, M., Udintsev, G.B. *et al.*, US Govt. Printing Office, Washington, DC.
- Scientific Party, 1984. Sites 552–553, in *Sites 552–553*, pp. 31–233, eds Roberts, D.G., Schnitker, D. *et al.*, US Govt. Printing Office, Washington, DC.
- Scientific Party, 1987. Site 642, *Proc. Ocean Drill. Program, Initial Rep.*, **104**, 53–213.
- Stewart, J., Watts, A.B. & Bagguley, J., 2000. Three-dimensional subsidence analysis and gravity modelling of the continental margin offshore Namibia, *Geophys. J. Int.*, **141**, 724–746.
- Talwani, M. & Eldholm, O., 1973. The boundary between continental and oceanic crust at the margin of rifted continents, *Nature*, **241**, 325–330.
- Teagle, D.A.H. & Alt, J.C., 1999. Data Report: alteration and vein log of holes 917A and 918D southeast Greenland margin, 149–153, in ,Larsen, H.C., ,Duncan, R.A., ,Allan, J.F. & ,Brooks, K., *Proc. ODP, Sci. Results*, **163**, (College Station, TX (Ocean Drilling Program).
- Tian, X. & Buck, W.R., 2016. The Role of Magmatic and Volcanic Loads in Generating Seaward Dipping Reflector Structures on Volcanic Rifted Margins 2016 Fall AGU Meeting, EOS.
- Watts, A.B., 1988. Gravity anomalies, crustal structure and flexure of the lithosphere at the Baltimore Canyon Trough, *Earth planet. Sci. Lett.*, **89**, 221–238.
- Watts, A.B. & Cox, K.G., 1989. The Deccan Traps: an interpretation in terms of progressive lithospheric flexure in response to a migrating load, *Earth planet. Sci. Lett.*, **93**, 85–97.
- Watts, A.B. & Fairhead, J.D. 1997. Gravity anomalies and magmatism at the British Isles continental margin, *J. geol. Soc. Lond.*, **154**, 523–529.
- White, R.S. *et al.*, 2008. Lower-crustal intrusion on the North Atlantic continental margin, *Nature*, **452**, 460–464.
- Yilmaz, O.Z., 2001. Deconvolution, in *Seismic Data Analysis: Processing, Inversion, and Interpretation of Seismic Data*, pp. 159–270, ed. Yilmaz, O.Z., SEG, Chap. 2.

## SUPPORTING INFORMATION

Supplementary data are available at [GJI](https://academic.oup.com/gji) online.

**Table S1:** Compilation of geometric SDR observations.

**Figure S1:** Histogram of acquisition year of cruises given in Table S1.

**Figure S2:** SDR dip versus year of acquisition (from Table S1).

**Figure S3:** SDR thickness versus year of acquisition (from Table S1).

**Figure S4:** Constant versus variable infill.

**Figure S5:** Jumps and breaks.

**Figure S6:** Velocity model and corresponding synthetic seismogram for final model.

Please note: Oxford University Press is not responsible for the content or functionality of any supporting materials supplied by the authors. Any queries (other than missing material) should be directed to the corresponding author for the article.